Journal of Rock Mechanics and Geotechnical Engineering 15 (2023) 1248–1262

Contents lists available at ScienceDirect

Journal of Rock Mechanics and Geotechnical Engineering

journal homepage: www.jrmge.cn

Full Length Article

Physics-based and data-driven modeling for stability evaluation of buried structures in natural clays

Fengwen Lai [a,b], Jim Shiau [c,*], Suraparb Keawsawasvong [d], Fuquan Chen [e], Rungkhun Banyong [d], Sorawit Seehavong [d]

[a] Institute of Geotechnical Engineering, Southeast University, Nanjing, 211189, China
[b] Faculty of Civil Engineering and Geosciences, Delft University of Technology, 2628 CN Delft, the Netherlands
[c] School of Engineering, University of Southern Queensland, Toowoomba, QLD, 4350, Australia
[d] Department of Civil Engineering, Thammasat School of Engineering, Thammasat University, Pathumthani, 12120, Thailand
[e] College of Civil Engineering, Fuzhou University, Fuzhou, 350116, China

ARTICLE INFO

Article history:
Received 16 March 2022
Received in revised form
13 May 2022
Accepted 17 July 2022
Available online 11 August 2022

Keywords:
Buried structures
Natural clays
Active trapdoor
Undrained stability
Multivariate adaptive regression splines (MARS)
Finite element limit analysis (FELA)

ABSTRACT

This study presents a hybrid framework to predict stability solutions of buried structures under active trapdoor conditions in natural clays with anisotropy and heterogeneity by combining physics-based and data-driven modeling. Finite-element limit analysis (FELA) with a newly developed anisotropic undrained shear (AUS) failure criterion is used to identify the underlying active failure mechanisms as well as to develop a numerical (physics-based) database of stability numbers for both planar and circular trapdoors. Practical considerations are given for natural clays to three linearly increasing shear strengths in compression, extension, and direct simple shear in the AUS material model. The obtained numerical solutions are compared and validated with published solutions in the literature. A multivariate adaptive regression splines (MARS) algorithm is further utilized to learn the numerical solutions to act as fast FELA data-driven surrogates for stability evaluation. The current MARS-based modeling provides both relative importance index and accurate design equations that can be used with confidence by practitioners.

1. Introduction

Natural clays more or less exhibit strength anisotropy wherewith the deposition and sedimentation processes follow preferred particle orientations. This is the so-called stress-induced anisotropy, where the anisotropic shear strengths are directionally dependent and are normally evaluated by undrained shear tests with varying major principal stress following its depositional axis.

Ladd (1991) and Ladd and DeGroot (2004) provided important data for the anisotropic undrained strength of clays under various shear modes. An empirical chart comparing undrained strengths obtained from triaxial compression (TC), triaxial extension (TE), and direct simple shear (DSS) as a function of the plasticity index of clay was also presented in Ladd and DeGroot (2004). Several researchers (Krabbenhøft and Lyamin, 2015; Ukritchon and Keawsawasvong, 2018a, 2019b; Krabbenhøft et al., 2019; Krabbenhøft, 2021) have proposed various failure criteria for modeling the undrained strength anisotropy of clays. These failure criteria are mostly formulated as a mathematical function of directionally dependent (anisotropic) undrained strength and orientation angle (δ) of the major principal stress (σ_1) to the depositional axis. The effects of anisotropic clay strengths on stability problems of various geotechnical infrastructures were extensively investigated, in particular for some buried structures, including tunnels (Wu et al., 2017, 2021; Keawsawasvong and Ukritchon, 2020, 2022; Chu et al., 2021; Man et al., 2022; Nguyen and Nguyen-Son, 2022), pipelines (Shiau and Hassan, 2021a, b; Tohidifar et al., 2021), and shallow/deep foundations (Rui et al., 2019; Ukritchon and Keawsawasvong, 2019a; Al-Naddaf and Han, 2021). Other published literature in relation to clay-based materials with anisotropic concerns could be found in Zhou et al. (2018) and Azarafza et al. (2019).

Terzaghi (1936) pioneered a study on failure mechanism and stress distribution above trapdoors in granular soils. Since then, trapdoor failures in active and passive modes have become an

* Corresponding author.
E-mail address: jim.shiau@usq.edu.au (J. Shiau).
Peer review under responsibility of Institute of Rock and Soil Mechanics, Chinese Academy of Sciences.

https://doi.org/10.1016/j.jrmge.2022.07.006

ongoing research field in geotechnical engineering. The active failure of a trapdoor correlates to its downward movement, resulting in a decrease in soil stress directly above it. Therefore, the active failure is extensively used for the stability analysis of subsurface pipelines subjected to ground support loss, roof collapse of subterranean spaces, tunnels, and mining operations (Suchowerska et al., 2012; Guan et al., 2017). In recent decades, considerable research on the stability of active trapdoors was conducted using a variety of techniques, including physical model tests (Costa et al., 2009; Iglesia et al., 2011, 2014; Al Heib et al., 2020; Costa and Zornberg, 2020), limit equilibrium method (Terzaghi, 1943), finite element analysis (Tanaka and Sakai, 1993; Hwang et al., 2005; Bhattacharya and Kumar, 2016; Lai et al., 2018; Ukritchon and Keawsawasvong, 2018b; Keawsawasvong and Ukritchon, 2019), and limit analysis (Wang et al., 2017; Lai et al., 2020, 2022; Keawsawasvong and Ukritchon, 2021; Yang et al., 2022).

Finite element limit analysis (FELA), as a novel, rigorous, and powerful numerical technique, has been widely used to investigate geotechnical stability problems. The upper bound (UB) and lower bound (LB) solutions provide accurate limit loads from above and below (Chen and Liu, 1990; Sloan, 2013; Oberhollenzer et al., 2018; Chen et al., 2020). This numerical technique is based on finite element discretization, plastic bound theorems (Drucker et al., 1952), and mathematical optimization. Sloan et al. (1990) and Martin (2009) used the FELA to establish benchmark solutions for active planar trapdoors inhomogeneous clays. The UB and LB solutions for planar and circular trapdoors in non-homogeneous clays with linearly increasing undrained shear strength were presented by Keawsawasvong and Ukritchon (2017) and Keawsawasvong and Shiau (2022). Furthermore, Wang et al. (2017) provided numerical UB and LB solutions for planar trapdoors in cohesive-frictional soils using the FELA and the discontinuity layout optimization (DLO) techniques. In recent years, for three-dimensional (3D) homogeneous and isotropic clays, Ukritchon and Keawsawasvong (2019c) and Shiau et al. (2021a, b) investigated the undrained stability of flat rectangular and square trapdoors using 3D FELA, whilst Shiau et al. (2022) studied the 3D effect of various cavity shapes.

It should be noted that the previous FELA investigations of buried structures under active trapdoors were limited to conditions with isotropic strengths utilizing Tresca or Mohr-Coulomb failure criteria, except for the work by Keawsawasvong and Ukritchon (2021), who presented LB solutions of active planar trapdoors in non-homogeneous and anisotropic clays obeying the Davis and Christian's (DC) failure criterion (Davis and Christian, 1971). The recent development of the anisotropic undrained shear (AUS) failure criterion in Krabbenhøft et al. (2019) has never been used to study the stability of active trapdoors in the past. Even though both DC and AUS failure criteria consider an empirical correlation of the undrained strength (s_u) of clay in DSS, TC and TE, the explicit form of the DC failure criterion cannot be applied to 3D problems since it was developed under plane strain condition. Unlike the DC model, the AUS model was developed under 3D coordinates which can be used to simulate two-dimensional (2D) and 3D (both plane strain and axisymmetric) problems. As a result, the AUS model is preferred in this paper to investigate the stability of circular trapdoors under axisymmetric conditions. Furthermore, only the LB solutions of plane strain trapdoor stability were presented in Keawsawasvong and Ukritchon (2021), while the UB solutions to the same problem have never been reported in the past.

The evaluation of the active failure of structures buried in natural clays using stability solutions from design charts is a manual and time-consuming process because it requires engineer to process soil parameters and geometric configurations and generate safety factor estimates in the preliminary design. Determining stability solutions using a data-driven surrogate is an expedient means of incorporating sophisticated numerical analyses into a design scheme to conduct stability evaluations. For buried structures under active trapdoor conditions (e.g. subjected to ground support loss or differential settlements), the data-driven surrogate allows stability evaluations to be done both efficiently and effectively. For such purpose, this study presents a hybrid framework for forecasting the undrained stability of active trapdoors in natural clays by integrating the benefits of both physics-based and data-driven models.

This paper aims to bridge the current research gaps by undertaking the rigorous UB/LB-FELA for undrained stability of both planar and circular trapdoors in natural clays simulated by the recently developed AUS failure criterion. The novel UB and LB solutions of stability number (N_{PS} and N_{AX}) are obtained and presented in the form of explicit design charts, which are a function of dimensionless parameters including trapdoor cover ratio, strength gradient, and anisotropic strength ratios. A numerical (physics-based) database of stability numbers derived from 294 separate analyses is then developed. A multivariate adaptive regression splines (MARS) model is employed to learn the numerical data to act as a fast FELA data-driven surrogate for implementation in preliminary design and during serviceability. The proposed relative importance index (RII) and MARS-based design equation of the current study would assist practitioners in evaluating trapdoor-related stability problems.

2. Problem statement

Trapdoor stability problems have long been an important research topic in geotechnical engineering. The active trapdoor can be applied to analyze the collapse of an underground roof in tunnels and mining works, the gravitational flow of granular material through hoppers, and the stability of buried pipes or anchors subjected to the loss of ground support. Fig. 1 shows the problem statement of both active planar and circular trapdoors in non-homogeneous clays with linearly increasing anisotropic shear strength. In a planar trapdoor, the geometry is very long, and it can be considered under plane strain condition; whereas the axisymmetric condition represents an actual 3D circular trapdoor even though it is analyzed in 2D axisymmetric condition. Centerline (C. L.) and axis of symmetry (A. O. S.) are utilized to represent symmetric or axisymmetric models, respectively. The planar or circular trapdoors with a width or a diameter (D) are situated beneath a clay layer with a cover depth (H). A cover ratio, denoted as H/D, can be defined here to represent the geometric configuration of trapdoors. A uniform surcharge (σ_s) is applied to the ground surface, while the support trapdoor pressure is denoted as (σ_τ). The active failure is triggered by allowing the trapdoor to slide downwards with the actions of overburden pressures σ_s and γH (γ is the unit weight of soils), which would be resisted by the action of the support stress σ_τ.

The trapdoor is assumed to be perfectly rigid, and the AUS failure criterion with the associated flow rule is used to establish the anisotropic clay failure criterion (Krabbenhøft et al., 2019). The three AUS strengths obtained from TC (s_{uc}), TE (s_{ue}), and DSS (s_{us}) are the input strengths of these failure criteria for FELA (see Fig. 1).

Therefore, two dimensionless anisotropic strength ratios can be defined as $r_e = s_{ue}/s_{uc}$ and $r_s = s_{us}/s_{uc}$ (Ladd, 1991; Krabbenhøft et al., 2019). According to Krabbenhøft et al. (2019), the relationship between r_e and r_s is introduced to determine the harmonic mean:

$$r_s = \frac{2r_s}{1 + r_s} \tag{1}$$

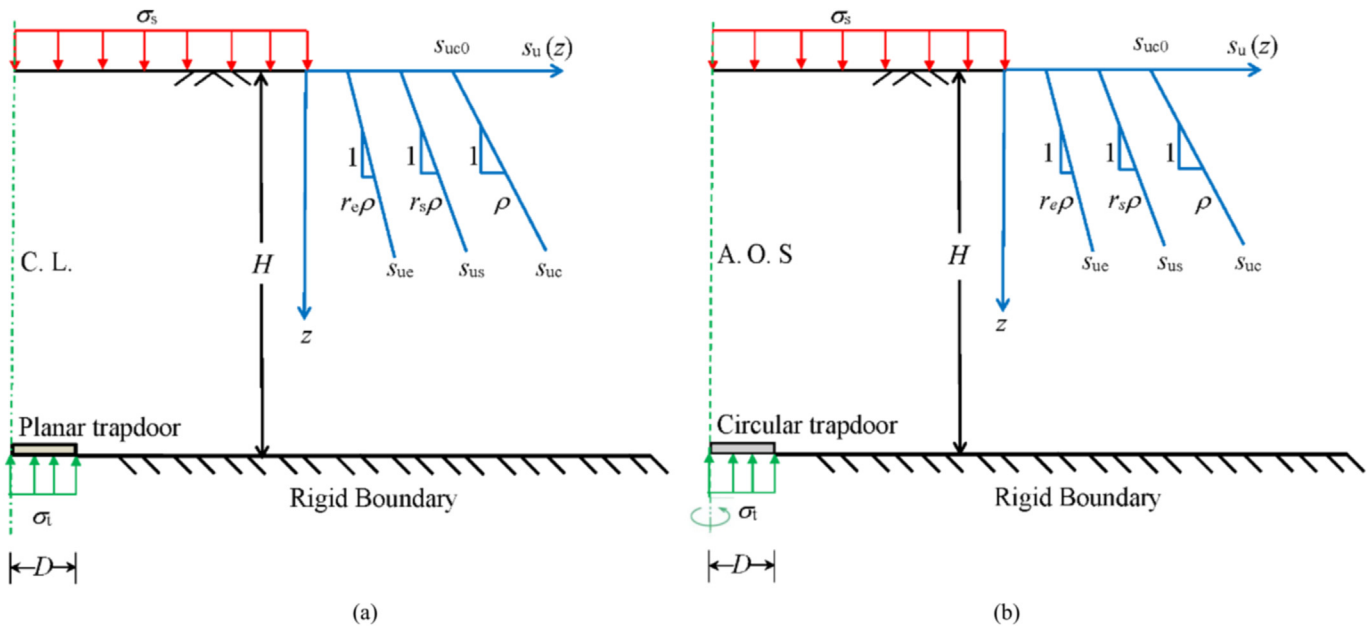

Fig. 1. The problem definitions in non-homogeneous and anisotropic clays: (a) Planar trapdoor and (b) Circular trapdoor.

Since r_s is a function of r_e, as shown in Eq. (1), r_e is the only anisotropic strength ratio employed in the parametric analysis. It is important to note that r_e has a range of 0.5–1 (Ladd, 1991; Krabbenhøft et al., 2019). Fig. 2 further demonstrates that r_e can affect the failure surface development of the AUS failure criterion. Note that the strengths in TC and TE in Fig. 2 are literally equal to $2s_{uc}$ and $2s_{ue}$, respectively. The form of the yield function of the AUS model with the harmonic mean of three undrained shear strengths can be expressed as

$$F_u = \sigma_1 - \sigma_3 + (r_e - 1)(\sigma_2 - \sigma_3) - 2s_{uc} = 0 \tag{2}$$

where $\sigma_1 \geq \sigma_2 \geq \sigma_3$ are the principal stresses (positive in compression) and F_u is the yield function. It is noted that the AUS failure criterion is being well transformed into the Tresca failure criterion by setting $r_e = 1$ (i.e. $s_{uc} = s_{ue} = s_{us}$).

Bishop (1966) experimentally showed that the undrained strength of normally consolidated and slightly over-consolidated clay increases approximately linearly with depth. Therefore, the three AUS strengths (s_{uc}, s_{ue}, and s_{us}) are assumed to be linearly increasing with depth and can be represented as

$$s_{uc}(z) = s_{uc0} + \rho z \tag{3}$$

$$s_{us}(z) = s_{us0} + r_s \rho z \tag{4}$$

$$s_{ue}(z) = s_{ue0} + r_e \rho z \tag{5}$$

where s_{uc0}, s_{ue0}, and s_{us0} are the AUS strengths at the ground surface; z is the depth measured from the ground surface; and ρ is the linear strength gradient. Note that the increasing rates of s_{uc0}, s_{us0}, and s_{ue0} are different and equal to ρ, $r_s\rho$, and $r_e\rho$, respectively, where $\rho \geq r_s\rho \geq r_e\rho$ (see Fig. 1).

The dimensionless approach was used to obtain the stability solutions of active planar and circular trapdoors in non-homogeneous clay with linearly increasing anisotropic shear strength. The considered parameters were simplified to three dimensionless input parameters (H/D, m, and r_e), which can be expressed as a function of the stability number:

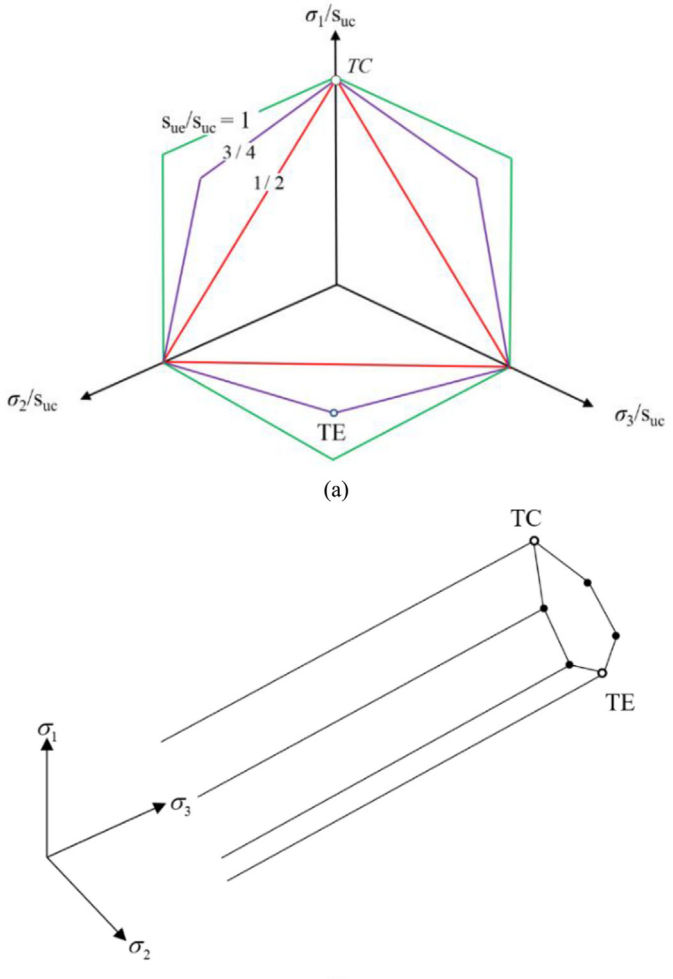

Fig. 2. Undrained strength envelopes of AUS model for different $r_e = s_{ue}/s_{uc}$ (after Krabbenhøft et al., 2019): (a) Planar trapdoor and (b) Circular trapdoor.

$$N_{PS} \text{ or } N_{AX} = \frac{\sigma_s + \gamma H - \sigma_t}{s_{uc0}} = f\left(\frac{H}{D},\ m,\ r_e\right) \quad (6)$$

where N_{PS} or N_{AX} represent the stability number of planar and circular trapdoors, which are the functions of the cover ratio H/D, dimensionless strength gradient ($m = \rho H/s_{uc0}$), and the anisotropic strength ratio r_e. The action of the resistance is represented by the negative sign in front of σ_t, whereas the positive sign of σ_s indicates the active movement of the driving stresses. Note that the adhesion factor defined at the contact between the plate element and surrounding soils varied from fully smooth to fully rough conditions. However, Keawsawasvong and Ukritchon (2017) and Keawsawasvong and Ukritchon (2021) found that there is no difference between the values of the stability numbers of both fully smooth and fully rough cases when H/D is less than 7. Also, when the H/D is greater than 7, the adhesion factor still has a smaller effect on the trapdoor stability since the difference between the cases of fully smooth and fully rough conditions is less than 2%–3.5%. Thus, to reduce the considered parameters and to avoid overfitting problems in the development process of data-driven surrogates, this study focuses on the case of fully rough conditions.

A practical range of parametric studies are chosen as follows: (a) cover ratio H/D = 0.5, 1, 2, 4, 6, 8, and 10; (b) strength gradient m = 0, 0.25, 0.5, 0.75, 1, 2, and 4; and (c) anisotropic strength ratio r_e = 0.5, 0.6, 0.7, 0.8, 0.9, and 1. The practical range of r_e may be conveniently estimated from the data of Ladd (1991), who proposed an empirical correlation between the undrained shear strength ratios in compression and extension as a function of the plasticity index of natural clays. Based on the Ladd (1991) data, the r_e ranges from 0.5 to 0.8 in practice. Thus, to cover a wider range, r_e = 0.5–1 will be used in following. It should be emphasized that r_e = 1 represents the case of isotropic clays. The findings by Won (2013) and Krabbenhøft et al. (2019) also confirmed this practical range. The degree of strength inhomogeneity is described by the dimensionless strength gradient. The characteristic of the clay and its geological process have a major influence on the s_{uc0} and ρ. According to Keawsawasvong and Ukritchon (2017) and Keawsawasvong and Shiau (2022), the dimensionless strength gradient is practically found in the range from 0 for a homogeneous clay to as high as m = 4 for the extreme combinations of these parameters.

3. Physics-based modeling

The stability number for planar and circular trapdoors in anisotropic and inhomogeneous clays with linearly increasing strengths is numerically determined using commercial software OptumG2 (Krabbenhøft and Lyamin, 2015). The use of both UB and LB together would significantly improve the confidence in the produced results using FELA (Sloan, 2013). In OptumG2, UB elements use six-node elements with continuous quadratic interpolation of unknown velocity, whereas LB elements use three-node elements with linear interpolation of unknown stresses, with stress discontinuities allowed at shared edges of neighboring triangles.

Fig. 3a and b shows the numerical models of planar and circular trapdoors under plain strain and axisymmetric conditions, respectively. The centerline of the problem is the symmetry line of the domain, which is positioned to the left boundary. Note that the model in Fig. 3a is under plane strain condition with the half of the domain, whereas that in Fig. 3b is under axisymmetric conditions in which the r–z section is employed and the line of axial symmetry is placed to the left of the domain. An AUS model with an accompanying flow rule represents the soil mass above the trapdoor. The trapdoor is modeled by rigid plate components with rough surface

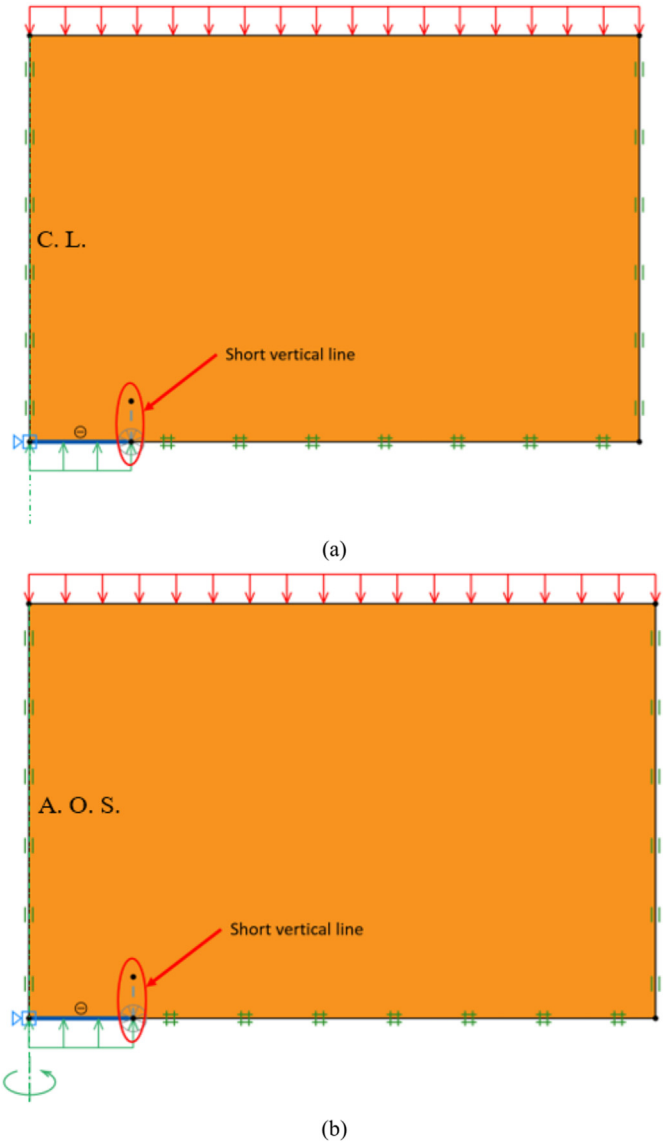

Fig. 3. Model domains for: (a) Planar trapdoor and (b) Circular trapdoor.

conditions. Since the edge of the trapdoor has obvious high stresses and velocity discontinuities, a short vertical line is introduced by employing interface elements and appended to the edge of the trapdoor as can be seen in Fig. 3a and b. The AUS strength of these interface elements is set to be 0. These vertical lines in Fig. 3a and b are essential in the UB analysis because velocity discontinuities are not permitted along all inter-element edges, but they are expected to occur at the corner of the trapdoor, which can significantly improve the correctness of the UB solutions. However, because stress discontinuities are simulated at all inter-element edges, this vertical line is unaffected by the precision of LB solutions.

The standard boundary conditions are enforced in all the FELA models. The bottom boundary of both models was fixed in both x and y directions, except where the trapdoor is located. The left (centerline) and the right boundaries were allowed to move in y-direction only. The domain size of both models was selected to be large enough so that the expansion of the overall velocity field has a neglectful effect on the solutions. To construct the tight UB and LB solutions, an autonomously adaptable mesh refinement was used in both the UB and LB simulations. Furthermore, adaptive mesh refinement with shear dissipation as a convergence criterion is

enabled to balance the computational accuracy and cost (Ciria et al., 2008). That is, the number of meshes will automatically increase in sensitive zones with significant plastic shearing strain, hence enabling users to more clearly and quickly identify the potential failure mechanisms. With an initial mesh number of 5000 elements and a final mesh number of 10,000 elements, five adaptive meshing stages were adopted throughout the study. It should be noted that the final adaptive meshes are utilized to show the failure mechanisms of the trapdoor in the paper. It is worth noting that more elements in the sensitive areas can lead to more correctness of the solutions. The staged procedure refers to the initial meshes to reach the target value. The number of elements and stages is large enough to neglect the effect on the solutions. Based on the suggestions by Krabbenhøft et al. (2015), the set of five iteration steps and mesh adaptivity increasing from 5000 to 10,000 elements is sufficient to produce the rigorous LB and UB solutions, where the differences between both bound solutions are less than 1% for all cases. To obtain the stability number N_{PS} and N_{AX}, the ultimate surface pressure (σ_s) is computed using LB/UB-FELA and then normalized by following the expression in Eq. (6).

4. Comparison and validation

To validate the computed FELA solutions, Fig. 4 compares the stability numbers (N_{PS} and N_{AX}) between the present and the previous studies for isotropic clays. Numerical results in Fig. 4a and b have shown excellent agreement between the present and the previous studies in isotropic clays with homogeneity or heterogeneity. Note that the present solutions used in the verifications in Figs. 4 and 5 are the average solutions from the UB and LU solutions obtained from OptumG2. Sloan et al. (1990) and Martin (2009)

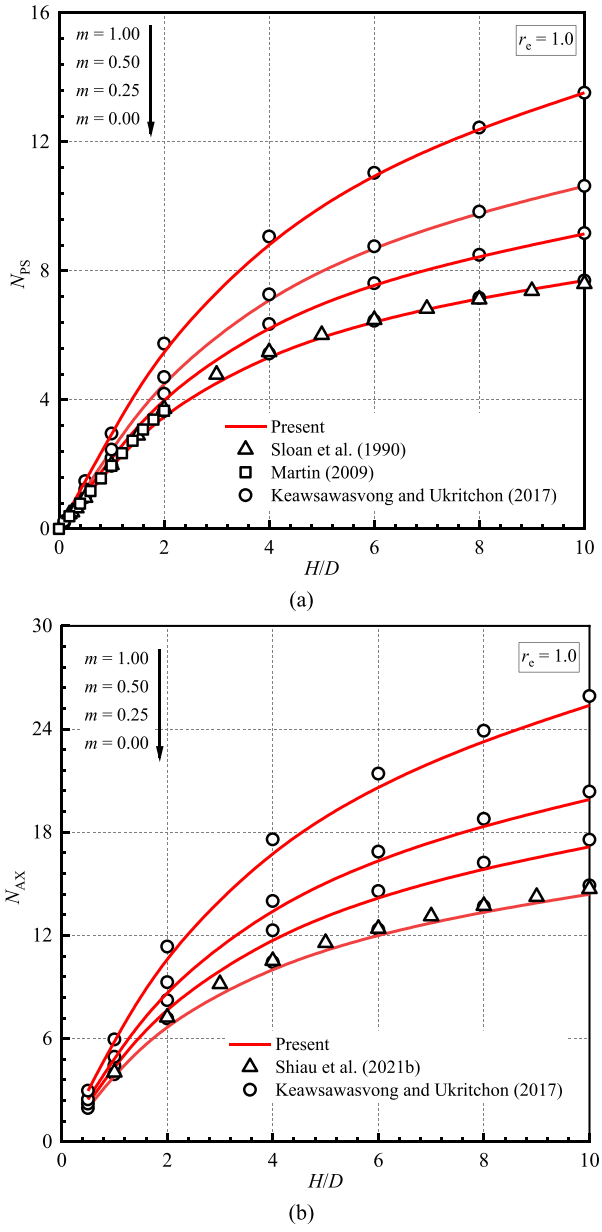

Fig. 4. Comparisons of the present study and previous studies for isotropic clays with $r_e = 1$: (a) Planar trapdoors and (b) Circular trapdoors.

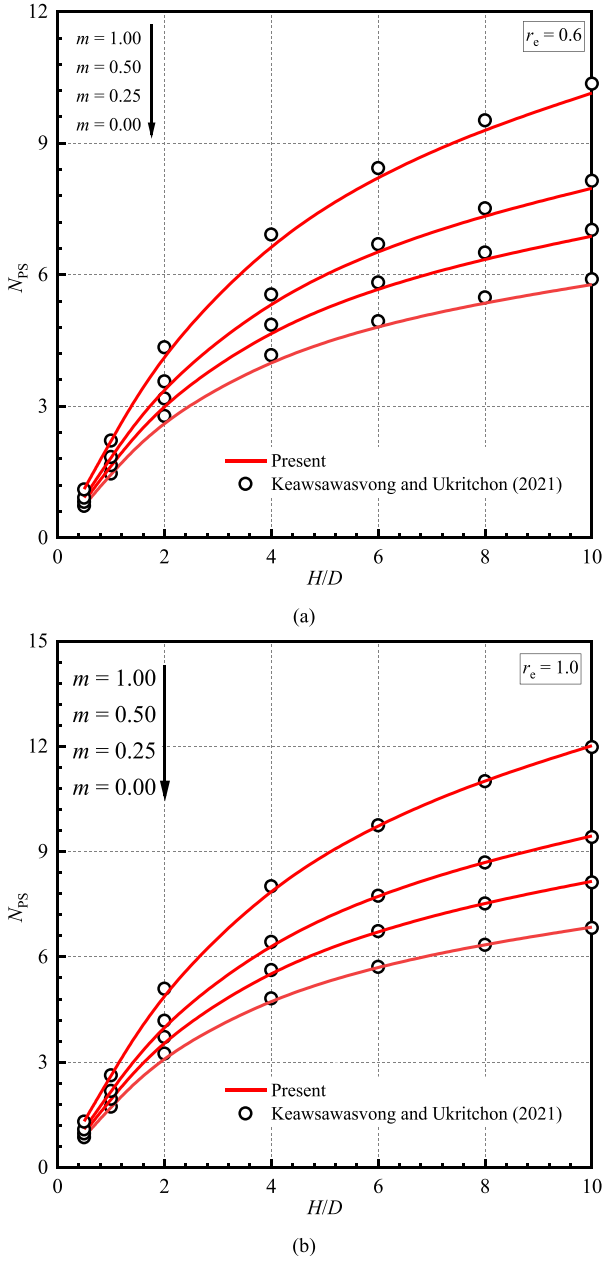

Fig. 5. Comparisons of the present study and previous studies for planar trapdoors in anisotropic clays with: (a) $r_e = 0.6$ and (b) $r_e = 0.8$.

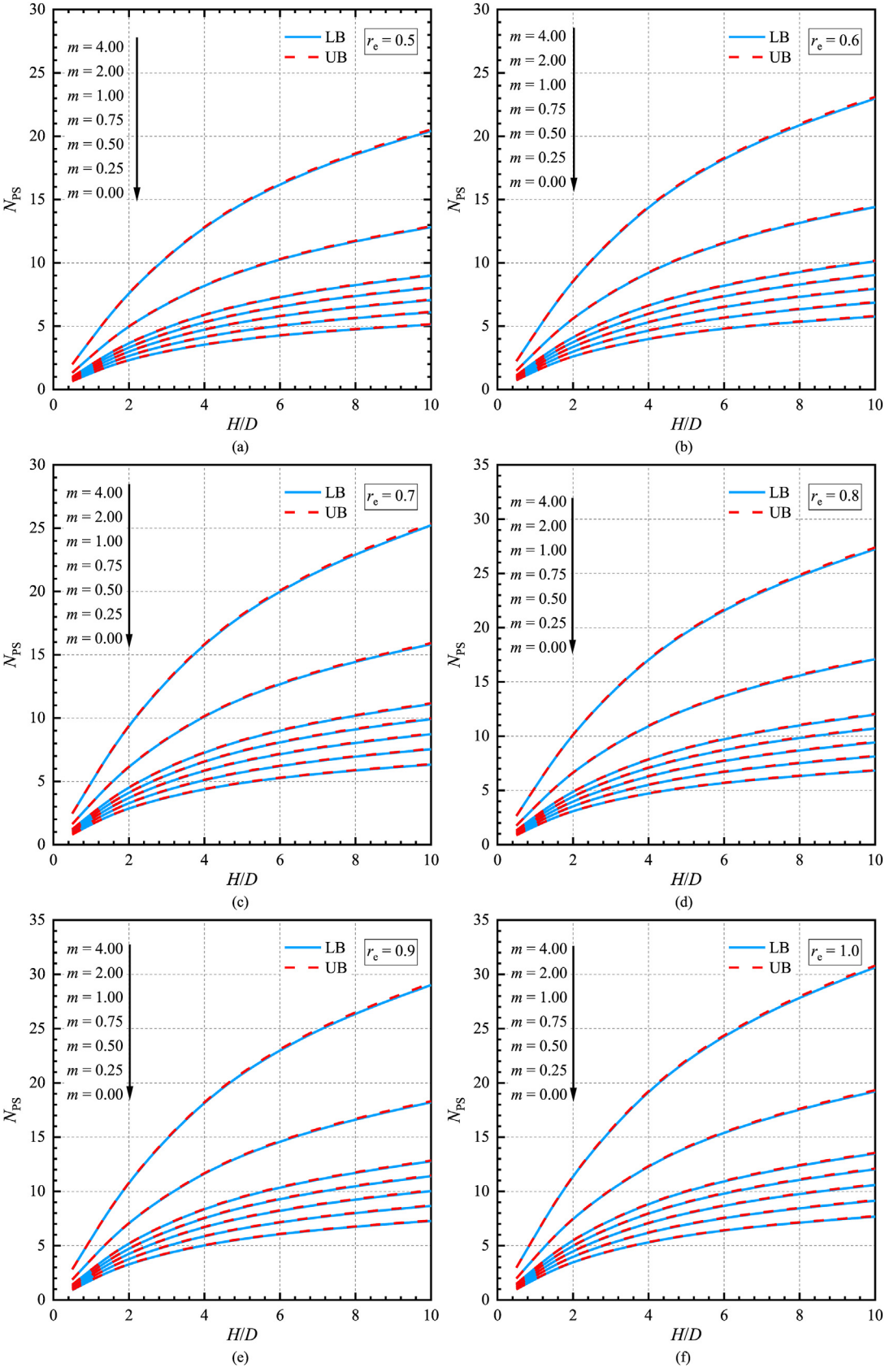

Fig. 6. Effect of H/D on N_{PS} of planar trapdoors in anisotropic and non-homogeneous clays with various r_e: (a) $r_e = 0.5$; (b) $r_e = 0.6$; (c) $r_e = 0.7$; (d) $r_e = 0.8$; (e) $r_e = 0.9$; and (a) $r_e = 1$.

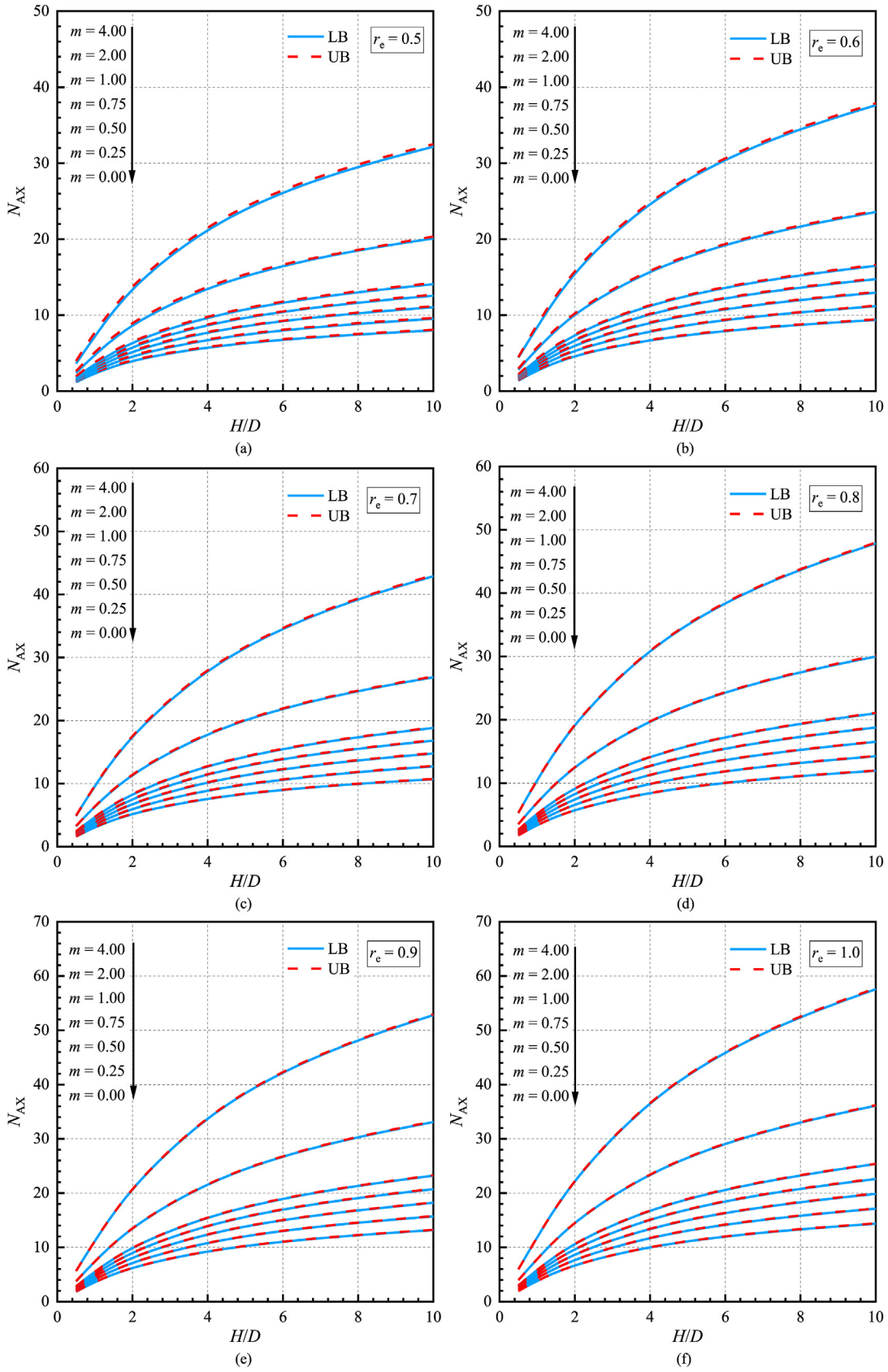

Fig. 7. Effect of H/D on N_{AX} of circular trapdoors in anisotropic and non-homogeneous clays with various r_e: (a) $r_e = 0.5$; (b) $r_e = 0.6$; (c) $r_e = 0.7$; (d) $r_e = 0.8$; (e) $r_e = 0.9$; and (a) $r_e = 1$.

presented the average FELA solutions of N_{PS} of planar trapdoors in isotropic and homogeneous clays ($m = 0$ and $r_e = 1$) under various cover ratios, while Keawsawasvong and Ukritchon (2017) reported those in the non-homogeneous clays with $m = 0$, 0.25, 0.5 and 1. For the circular trapdoors, Keawsawasvong and Ukritchon (2021) and Shiau et al. (2021b) obtained the FELA solutions in isotropic and homogeneous clays under 2D and 3D conditions. It should be noted that these previous works are limited to the cases of trapdoors in isotropic clays obeying the Tresca failure criterion, which is only equivalent to the cases of $r_e = 1$. Their solutions cannot be applied to the cases of anisotropic strengths with $r_e \neq 1$ which will be presented later in this paper by using the AUS failure criterion. As a result, Fig. 4 confirms the correctness of using the AUS model with $r_e = 1$ to simulate the geotechnical problems in consideration of the Tresca model.

The comparisons of stability number (N_{PS}) of planar trapdoors embedded in anisotropic clays modeled using the DC model by Keawsawasvong and Ukritchon (2021) and the AUS model by the present study are shown in Fig. 5 for the cases of $r_e = 0.6$ and 0.8, respectively. Note that these cases represent the trapdoor stability in conjunction with the anisotropic strengths, where all the AUS strengths s_{uc}, s_{ue}, and s_{us} are considered. Unlike the Tresca model, it has only the isotropic undrained shear strength of s_{uc}. In addition, only the problem of plane strain trapdoor is compared here as the DC model cannot realistically model the natural clays with heterogeneity and anisotropy under the axisymmetric condition. Under various strength gradients (m), the present studies are in good agreement with the previous studies, showing that using the AUS model can provide almost the same results as the DC model. According to Fig. 5, the solutions of plane strain trapdoors with the AUS model are in good agreement with those with the DC model, which confirms the correctness of the use of the AUS model to derive the stability solutions of anisotropic clays under plane strain condition.

It should be noted that the DC envelope proposed by Davis and Christian (1971) was developed under the plane strain condition, where an anisotropic undrained strength of clay is expressed in terms of the plane strain state of stress (σ_{xx}, σ_{zz}, τ_{zx}) in the x–z plane, and therefore it cannot be used to investigate the stability of 3D or axisymmetric problems (Ukritchon and Keawsawasvong, 2018a, 2020; Ukritchon et al., 2019). The AUS model is superior to the DC model since the AUS model was formulated in terms of the general 3D Cartesian state of stress (σ_{xx}, σ_{yy}, σ_{zz}, τ_{xy}, τ_{yz}, τ_{zx}) so that it can be applied to 3D problems like circular or rectangular trapdoors in anisotropic clays.

5. Numerical results and discussions

Figs. 6 and 7 show the effects of cover ratios (H/D) on the stability number (N_{PS} and N_{AX}) of planar and circular trapdoors in anisotropic and non-homogenous clays, respectively. These figures are also the design charts, as they comprehensively illustrate the variations in N values with H/D under various m values for the cases of r_e = 0.5, 0.6, 0.7, 0.8, 0.9, and 1 in planar and circular trapdoor problems. In the figures, the dashed and solid lines represent the LB/UB-FELA solutions, respectively. It follows from Fig. 6 that, for the planar trapdoor problem, the N_{PS} value increases rapidly in the parabolic shape with H/D. It means that larger cover ratio can enhance the stability because of more stable arching effect. Moreover, the curvature of N_{PS} and H/D relationship is larger for higher m and r_e values. Similar phenomena can be also found in the circular trapdoor problem (see Fig. 7). The comparisons of N_{PS} and N_{AX} between Figs. 6 and 7 further indicate that, for the fixed dimensionless parameter groups, the N_{AX} of the circular trapdoor is larger than that of the planar trapdoor, which is attributed to the associated failure mechanisms that will be discussed later. The average results of N_{PS} and N_{AX} from UB and LB solutions are summarized in Tables. A1 and A2 in Appendix, respectively.

The effects of strength gradients (m) on stability number (N_{PS} and N_{AX}) of planar and circular trapdoors in anisotropic and non-homogeneous clays are explored with r_e varying from 0.5 to 1 in Fig. 8. A moderate cover ratio of $H/D = 2$ is chosen here. A linear correlation between N and m can be obviously observed in the figure for all studied cases. The underlying reason might be the assumption of undrained clays with linearly increasing strengths with depth. The change is more sensitive for the higher r_e (more homogeneous clays). In addition, the larger N_{AX} value of circular trapdoors than that of planar ones for a specific case can be found by comparing Fig. 8a and b.

The effects of anisotropic strength ratio (r_e) on stability number (N_{PS} and N_{AX}) of planar and circular trapdoors covered by

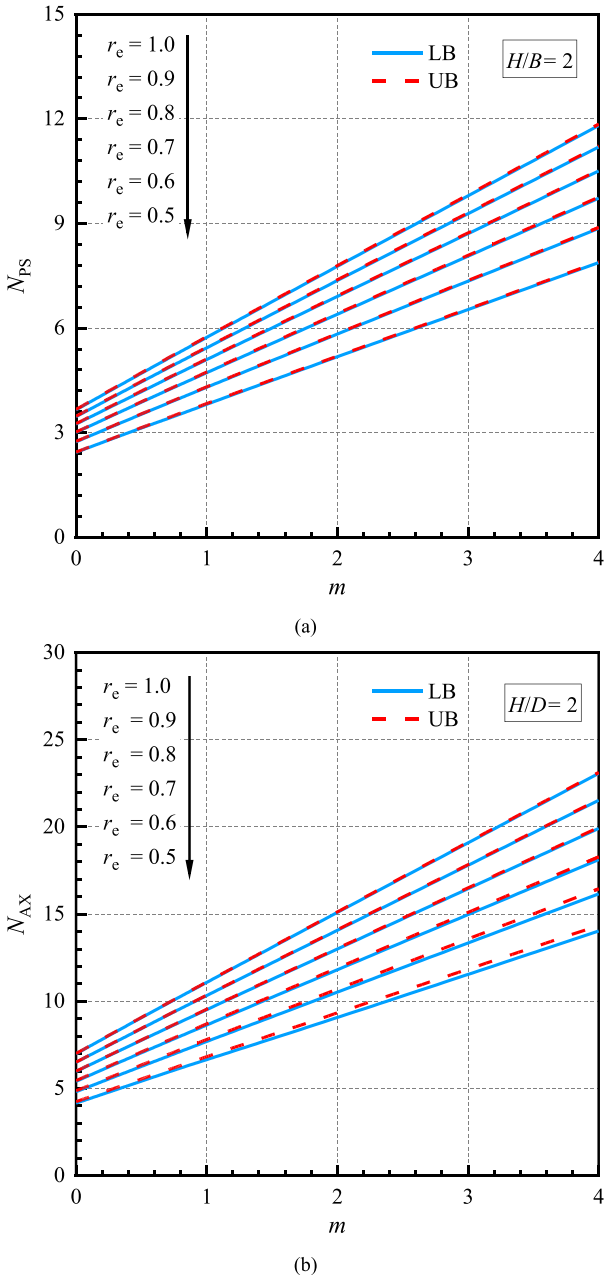

Fig. 8. Effect of m on N_{PS} and N_{AX} for: (a) Planar trapdoors and (b) Circular trapdoors.

anisotropic and non-homogeneous clays are shown in Fig. 9 for the cases of $m = 0$, 0.25, 0.5, 0.75, 1, 2, and 4. It is generally acknowledged that $s_{ue} \leq s_{us} \leq s_{uc}$, and s_{us} tends to be somewhat closer to s_{ue} than to s_{uc} in AUS model. It can be thus concluded that the N value increases nonlinearly with increasing anisotropic strength ratio at a given m value, implying that a lower degree of strength anisotropy gives rise to a higher stability number.

To further investigate the difference in stability performance between planar and circular trapdoors, a shape factor is defined as follows:

$$F = N_{AX}/N_{PS} \tag{7}$$

Fig. 10 shows the variation in the shape factor of trapdoor problems in anisotropic and non-homogenous clays under various H/D with $m = 0$, 1, and 4 for two cases of $r_e = 0.5$ and 0.8. It follows from Fig. 10 that the shape factor decreases with increasing cover ratio and/or decreasing strength gradient. Note that the influence of H/D on the shape factor is more significant for a higher degree of strength anisotropy. Moreover, the obvious difference between UB and LB solutions can be also seen for the lower values of r_e. It can therefore be concluded that both strength anisotropy and strength heterogeneity would result in significant shape effect for active trapdoor problems, especially for shallow trapdoors.

Fig. 11 presents the effects of cover ratio H/D on the failure mechanisms of active planar and circular trapdoors with $r_e = 0.7$ and $m = 1$, respectively. It shows the evolution of failure pattern of trapdoors in anisotropic and non-homogeneous clays from $H/D = 0.5$ (shallow trapdoor) to $H/D = 10$ (deep trapdoor). The failure pattern is visualized and interpreted in the form of automatically-adaptive meshes where the shear zone is concentrated. For $H/D \leq 2$, a nearly-vertical slip failure can be observed extending from trapdoor width to the ground surface. A possible reason for this is the lacking of soil arching above the trapdoor to transfer vertical

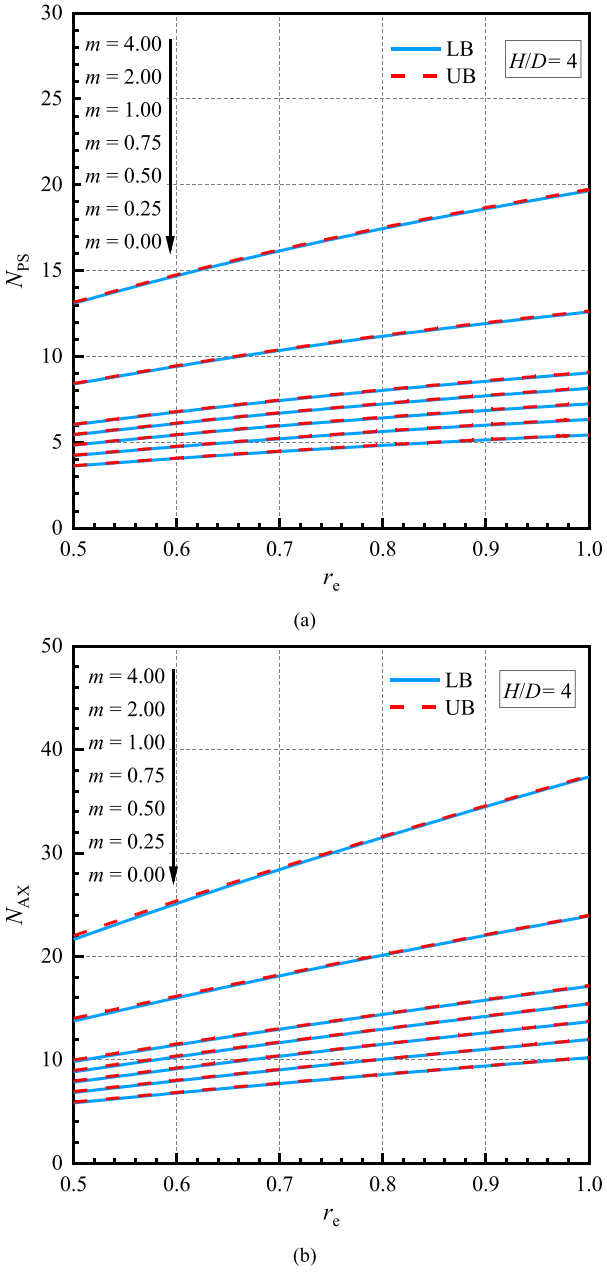

Fig. 9. Effect of r_e on N_{PS} and N_{AX} for: (a) Planar trapdoors and (b) Circular trapdoors.

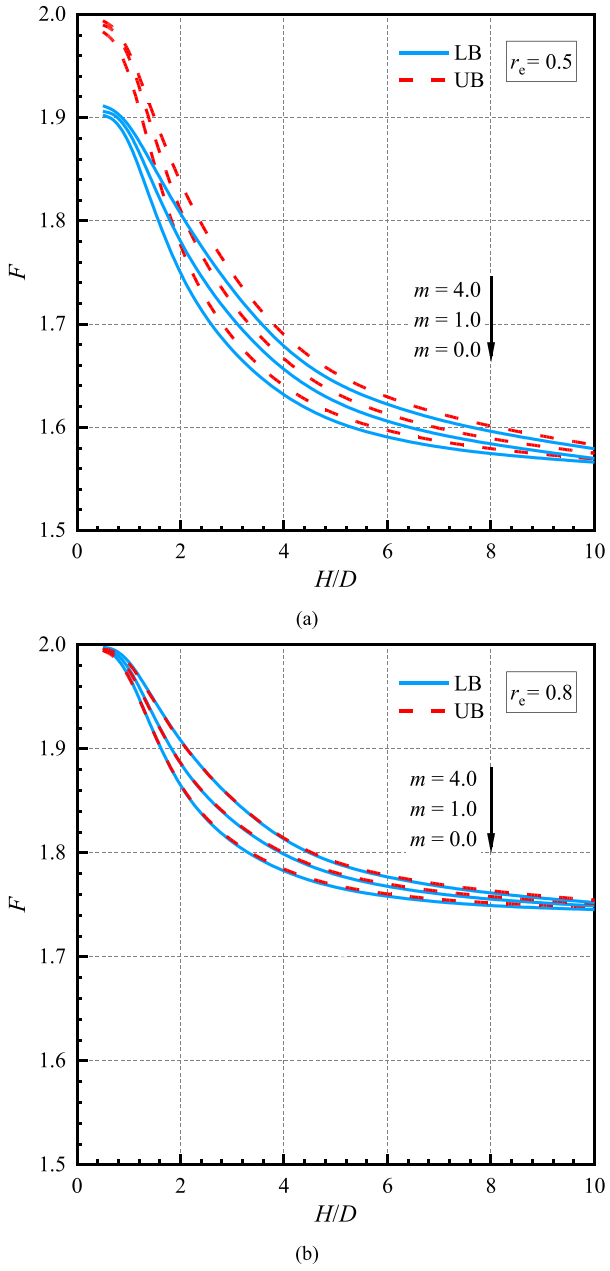

Fig. 10. Shape factor ($F = N_{AX}/N_{PS}$) for the cases of: (a) $r_e = 0.5$ and (b) $r_e = 0.8$.

loading, hence forming an instantaneous and integral collapse. This failure pattern typically needs to be avoided in practice. On the other hand, under the arching effect, the curvilinear (spiral) slip surfaces gradually develop outside the trapdoor corner and then intersect with the ground surface when $H/D > 2$. Therefore, same as the other research (Costa et al., 2009; Lai et al., 2018, 2020), $H/D = 2$ can be adopted as a depth ratio that distinguishes the shallow and deep trapdoors. It is of interest that, as the cover ratio increases, more clays are involved in plastic zones to resist a driving force, implying that a higher N_{AX} value will be obtained, as shown in Fig. 7. Such a phenomenon can be explained by the fact that a higher cover ratio induces more mobilized shear stress along a longer slip surface to form a larger plastic zone for resisting downward failure. Furthermore, when comparing the planar and circular trapdoors (see Fig. 11a and b), the circular trapdoor has a larger collapsed zone than the planar one at a fixed H/D, giving supporting evidence for the previous discussions on shape effects.

Fig. 12 presents the effect of strength gradient m on the failure mechanisms of active planar and circular trapdoors embedded in anisotropic and non-homogeneous clays with $r_e = 0.8$ and $H/D = 4$, respectively. Although the curvilinear slip surface can be also found in deep trapdoors for various m values, some differences are still observed: the larger the m value (soil strength), the smaller the width of the plastic zone. The discrepancy in the collapse zone extent between planar and circular trapdoors can be also found in Fig. 12.

Fig. 13 shows the effects of anisotropic strength ratios on the pattern of failure mechanism with $H/D = 6$ and $m = 0$. The differences in failure patterns are small both for planar and circular trapdoors, showing that the effect of anisotropy in developing the associated failure mechanism is insignificant. Even so, the effects on the stability of trapdoors cannot be neglected as a larger r_e value gives rise to a greater stability number (see Fig. 9). This finding is similar to the work in Keawsawasvong and Ukritchon (2021) where the DC model was used.

6. Development of data-driven surrogate

6.1. Numerical database and sensitivity analysis

The coupling effects of dimensionless design parameters on undrained stability of trapdoor problems were investigated in the previous section. It was found that the stability number poses a nonlinear and multi-dimensional relation with the input dimensionless design parameters. To provide a guideline for the preliminary design of trapdoor problems, the associated sensitivity analysis is vital to quantitatively assess the relative importance of each dimensionless design parameter. Moreover, even though we have presented a series of new dimensionless design charts in terms of stability number (discrete value) for most practical applications, geo-engineers still need to resort to interpolations for

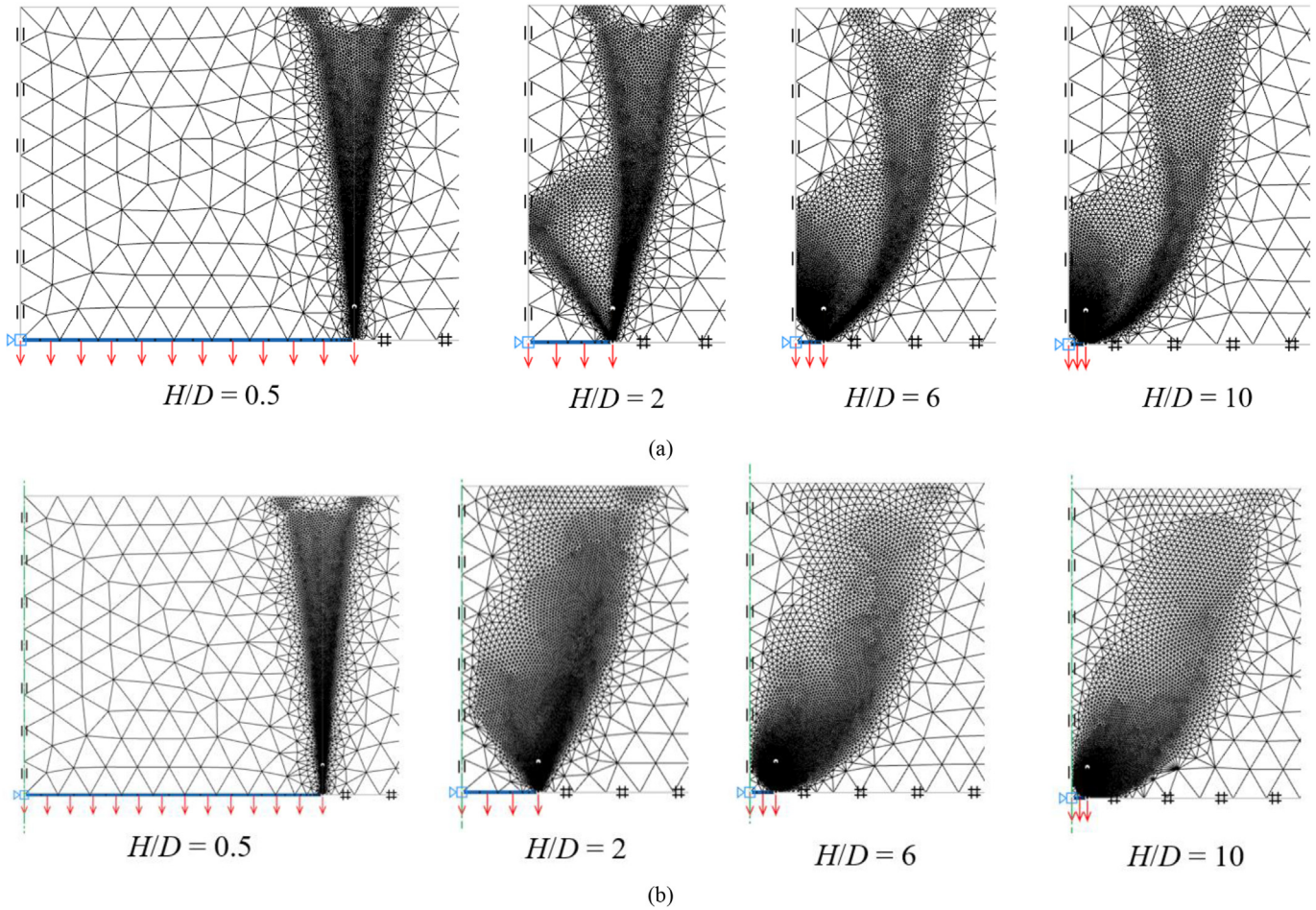

Fig. 11. Effect of H/D on failure mechanisms for planar and circular trapdoors with $r_e = 0.7$ and $m = 1$: (a) Planar trapdoors and (b) Circular trapdoors.

estimating other dimensionless parameters that do not match with those discrete ones.

Traditional nonlinear regression analysis used for empirical prediction typically requires presupposing the expressions of empirical equations before fitting, which leads to great uncertainties and challenges in its implementation. Moreover, for the multivariate problems, using the traditional nonlinear fitting techniques always cannot get a satisfying result with enough accuracy for practical use. To address this inconvenience, empirical prediction is an attractive alternative. The MARS model introduced in this paper is a nonparametric and nonlinear statistical regression method that can capture the underlying functional relationship among the input and output variables in high dimensions and their interactions without requiring any prior assumption (Friedman, 1991). Recently, the MARS model has been successfully used in a variety of geotechnical engineering problems, including the prediction of collapse potential for compacted soils, performances of deep excavations/shafts and tunnels, pile drivability, assessment of soil liquefaction, and stability analysis of pile-supported embankment (Zhang et al., 2017; Zhang, 2020; Zheng et al., 2020; Lai et al., 2021; Zhou et al., 2021).

The MARS model is operated by two major steps, i.e. forward and backward iterative steps. In the forward step, the model is generated by a cluster of basic functions (BFs, splines) that can be linearly connected by the knots. It can be written as follows:

$$BF = \max\ (0,\ x-t) = \begin{cases} x-t & (\text{if } x > t) \\ 0 & (\text{otherwise}) \end{cases} \tag{8}$$

where x is an input variable and t is a threshold value. The BFs provide greater flexibility for the model to allow the bends, thresholds, and other departures in linear functions to be considered. The MARS algorithm is to identify every possible predictor and potential knot location for every predictor. The global model (i.e. predictive target) can be thus expressed using the linear combinations of BFs:

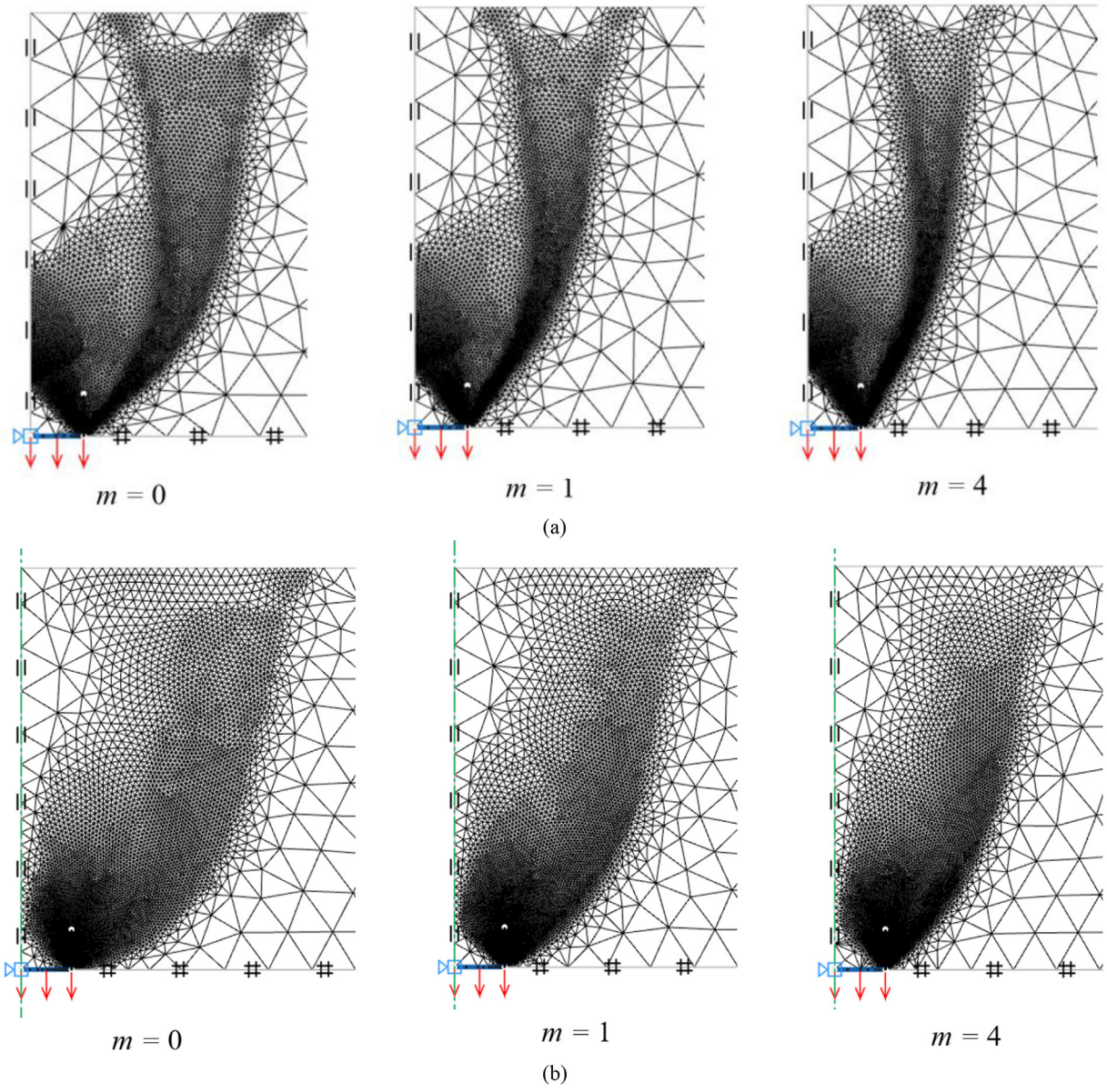

Fig. 12. Effect of m on failure mechanisms for planar and circular trapdoors with $r_e = 0.8$ and $H/D = 4$: (a) Planar trapdoors and (b) Circular trapdoors.

$$f(X) = \beta_0 + \sum_{m=1}^{M} \beta_m \lambda_m(X) \tag{9}$$

where β_0 is the constant, M is the amount of BFs, m is the number of each basis functionλ_m, and the coefficient β_m is a constant, which can be estimated with the least-squares approach. The BFs cover a given domain of the database in MARS.

The forward phase adds functions and finds potential knots to improve the performance of the training model, in spite of the likelihood to over-fitting model using Eq. (9) and various numbers of BFs. To obtain an optimal predicting function, the second step, known as the backward phase to prune the least effective terms is necessary. The unique back-pruning process effectively avoids the problem of overfitting, which is one of the most outstanding advantages of the MARS model, as compared to other traditional machine learning approaches (e.g. artificial neural network). In the second step, the backward pruning algorithm is employed to delete the redundant BFs with the least contributions, as assessed by the generalized cross-validation (GCV) value. Note that GCV value is a mean squared residual error divided by a penalty that is relevant to the model complexity, which can be obtained from a variance decomposition procedure:

$$GCV = \frac{\frac{1}{K}\sum_{i=1}^{K}[y_i - f(x_i)]^2}{\left[1 - \frac{M + d(M-1)/2}{K}\right]^2} \tag{10}$$

where K is the number of data points, d is the penalty factor, and $f(x_i)$ is the predicted value from the MARS model. The $(M\text{-}1)/2$ is the number of knots. Therefore, the GCV value is penalized by the M and N to reduce the probability of overfitting as much as possible. A default value of $d = 3$ is input in the MARS model. At each pruning step, the corresponding BF will be removed to minimize the GCV value until an optimal model is achieved. After that, the RII of each input variable on the output is generated by identifying the decrease in GCV value. Note that the RII value shows the importance level (sensitivity) for an output variable, and an RII of 100% represents that the corresponding input variable has the most significant effect on the output.

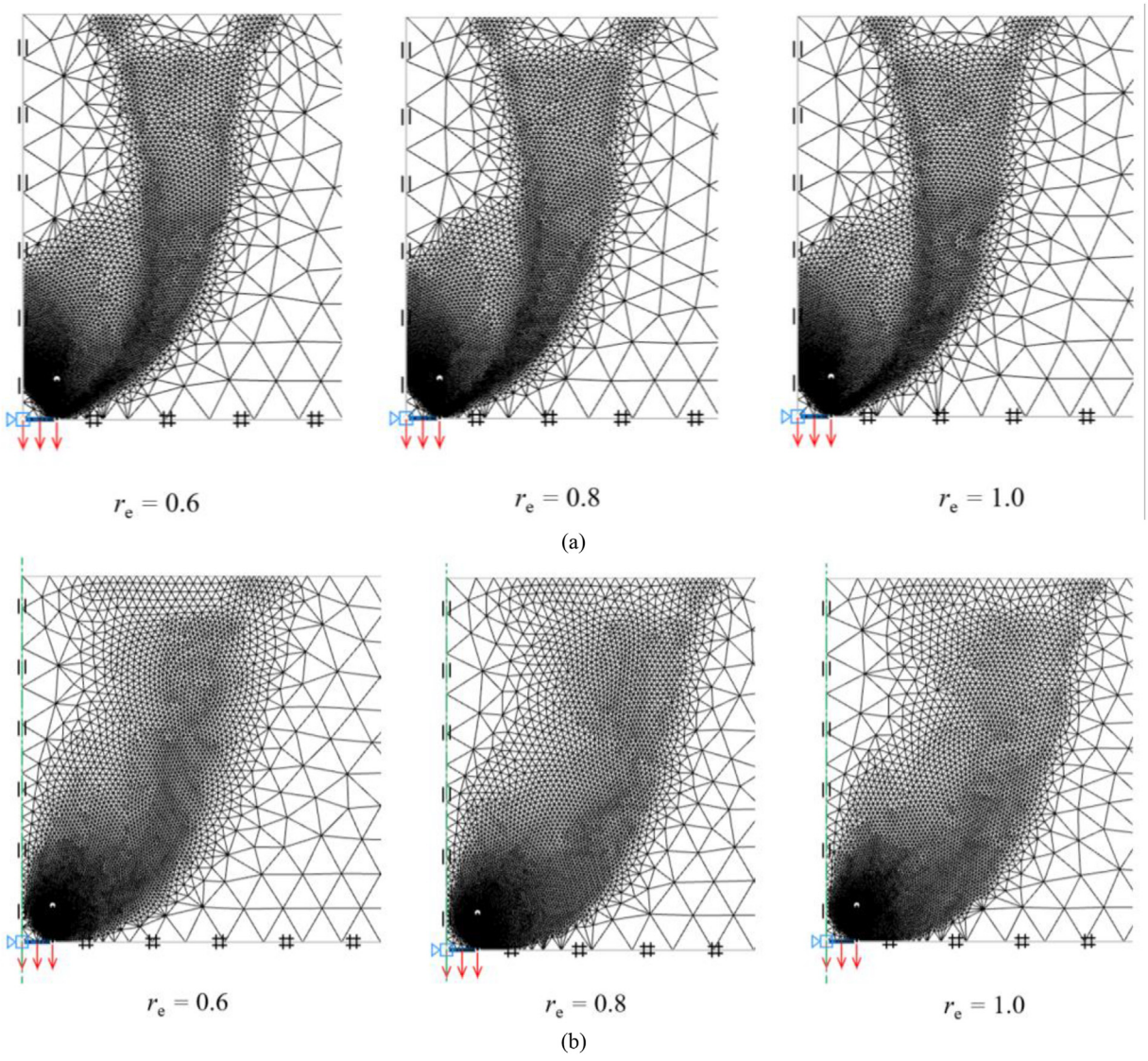

Fig. 13. Effect of r_e on failure mechanisms for planar and circular trapdoors with $H/D = 6$ and $m = 0$: (a) Planar trapdoors and (b) Circular trapdoors.

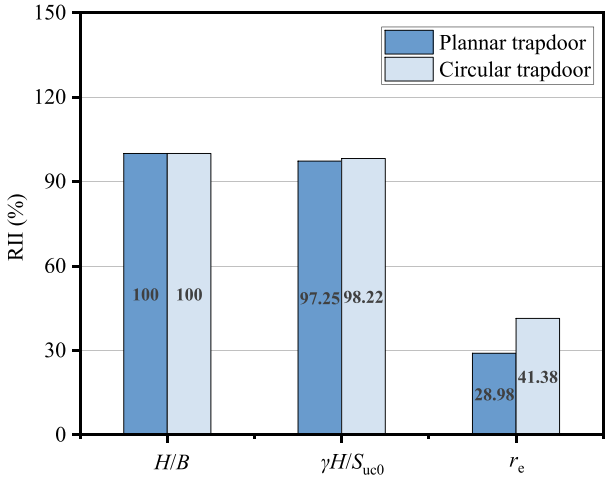

Fig. 14. RII of each input variable on stability number for planar and circular trapdoors.

In this study, 294 groups of average stability numbers (N_{PS} and N_{AX}) of planar and circular trapdoors in anisotropic and non-homogeneous clays are collected from FELA as the artificial datasets to run the MARS model. The datasets are shown in Tables A1 and A2 in the Appendix. In the MARS model, three design parameters (H/D, m, r_e) are chosen as input variables, while N_{PS} or N_{AX} are chosen as output variables. Note that the adhesion factor representing the interface roughness between the plate and the surrounding soils is not taken into account in the MARS model as its effect on the stability number is neglectable (Keawsawasvong and Ukritchon, 2017, 2021). The applications of MARS do not take this adhesion factor into account since the difference between rough and smooth cases is very small. It is also beneficial to construct a simpler model with minimal variables, seeking a balance between model complexity and performance. The calculated RII of each input variable is shown in Fig. 14. It can be found that the cover ratio H/D has the most significant influence on the N values of planar and circular trapdoors, followed by m and r_e. Noting that the soil strength gradient m has equal importance as the cover ratio H/D, the influence of anisotropy (r_e) on the stability is nevertheless relatively low, despite that it cannot be ignored.

6.2. MARS-based design equations

Using the data in Tables 1 and 2, two optimally-fitted design equations are presented to predict the stability number of planar and circular trapdoors, respectively.

Table 1
Basis functions and mathematical equations in MARS model for N_{PS} of planar trapdoors.

BF	Equation	*BF*	Equation
*BF*1	max(0, $H/D-4$)	*BF*13	max(0, $H/D-2$)
*BF*2	max(0, $4-H/D$)	*BF*14	max(0, $H/D-8$) *BF*11
*BF*3	max(0, $m-0$) *BF*1	*BF*15	max(0, $8-H/D$) *BF*11
*BF*4	max(0, $m-0$)	*BF*16	max(0, $H/D-8$) *BF*9
*BF*5	max(0, $H/D-2$) *BF*4	*BF*17	max(0, $8-H/D$) *BF*9
*BF*6	max(0, $2-H/D$) *BF*4	*BF*18	max(0, $H/D-6$)
*BF*7	max(0, $r_e-0.7$) *BF*5	*BF*19	max(0, $r_e-0.8$) *BF*13
*BF*8	max(0, $r_e-0.8$)	*BF*20	max(0, $0.8-r_e$) *BF*14
*BF*9	max(0, $0.8-r_e$)	*BF*21	max(0, $r_e-0.7$) *BF*3
*BF*10	max(0, $r_e-0.5$) *BF*2	*BF*22	max(0, $0.7-r_e$) *BF*3
*BF*11	max(0, $r_e-0.5$) *BF*4	*BF*23	max(0, $r_e-0.6$) *BF*4
*BF*12	max(0, $H/D-6$) *BF*4	*BF*24	max(0, $H/D-8$)

Table 2
Basis functions and mathematical equations in MARS model for N_{AX} of circular trapdoors.

BF	Equation	*BF*	Equation
*BF*1	max(0, $H/D-4$)	*BF*13	max(0, $H/D-4$) *BF*3
*BF*2	max(4 − H/D, 0)	*BF*14	max(0, $H/D-1$)
*BF*3	max(0, $m-0$)	*BF*15	max(0, $r_e-0.5$) *BF*5
*BF*4	max(0, $H/D-2$) *BF*3	*BF*16	max(0, $H/D-8$) *BF*3
*BF*5	max(0, $2-H/D$) *BF*3	*BF*17	max(0, $8-H/D$)
*BF*6	max(0, $r_e-0.5$) *BF*4	*BF*18	max(0, $H/D-2$)
*BF*7	max(0, $r_e-0.5$)	*BF*19	max(0, $r_e-0.9$) *BF*13
*BF*8	max(0, $H/D-6$) *BF*7	*BF*20	max(0, $0.9-r_e$) *BF*13
*BF*9	max(0, $6-H/D$) *BF*7	*BF*21	max(0, $H/D-6$) *BF*3
*BF*10	max(0, $H/D-2$) *BF*7	*BF*22	max(0, $r_e-0.7$)
*BF*11	max(0, $r_e-0.7$) *BF*3	*BF*23	max(0, $r_e-0.5$) *BF*17
*BF*12	max(0, $0.7-r_e$) *BF*3		

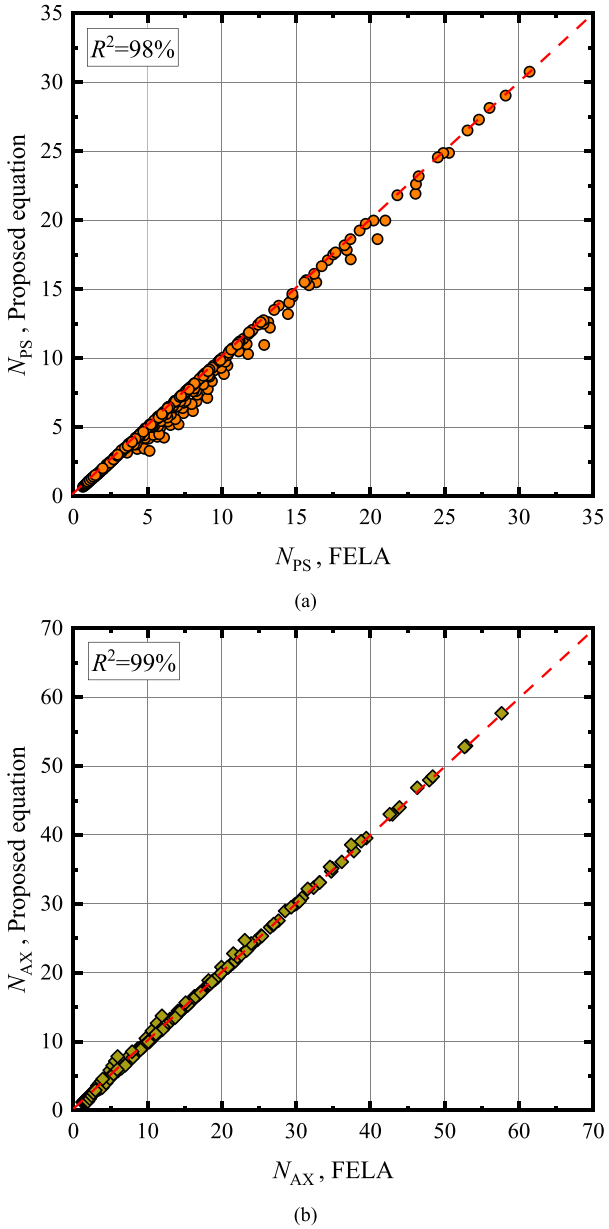

Fig. 15. Comparison of the N value between the proposed MARS equation and FELA: (a) Planar trapdoors and (b) Circular trapdoors.

$$N_{PS} = 6.634 + 1.299BF1 - 1.507BF2 - 0.242BF3 + 1.361BF4 + 0.502BF5 - 0.697BF6 - 0.31BF7 + 2.46BF8 - 10.005BF9 - 0.459BF10 + 5.898BF11 - 0.123BF12 - 0.856BF13 + 0.493BF14 - 0.69BF15 - 1.052BF16 + 1.035BF17 - 0.121BF18 + 0.212BF19 + 0.786BF20 - 0.106BF21 + 0.337BF22 - 0.466BF23 - 0.087BF24 \quad (11)$$

$$N_{AX} = 10.187 + 1.997BF1 - 2.567BF2 + 3.402BF3 + 0.715BF4 - 1.251BF5 + 1.195BF6 + 17.724BF7 + 1.91BF8 - 2.839BF9 - 1.501BF10 + 3.794BF11 - 4.43BF12 - 0.477BF13 - 0.844BF14 - 1.368BF15 - 0.107BF16 - 0.8BF18 - 0.766BF19 + 0.668\ BF20 - 0.18BF21 - 1.055BF22 - 0.171BF23 \quad (12)$$

To demonstrate the accuracy of proposed MARS-based design equations, numerical comparisons of N_{AX} and N_{PS} between the predicted and average UB/LB-FELA solutions are shown in Fig. 15. The predicted values of N_{AX} and N_{PS} are in good agreement with those of average FELA solutions, with the determination coefficient (R^2) of 98% and 99%. It can therefore be concluded that the proposed MARS-based design equations are accurate, and they can be used in practice with great confidence.

7. Conclusions

This study has successfully evaluated the stability of buried structures under active planar and circular conditions in anisotropic and non-homogeneous clays using a hybrid approach combining physics-based and data-driven modeling. Directionally dependent strengths (anisotropy) of clays were characterized by strengths compression, extension, and DDS with the newly-developed AUS model in the FELA code. The heterogeneity study of undrained clays was that the strength increases linearly with depth. Numerical results presented here were also compared with published solutions to validate the accuracy of the AUS model for isotropic and anisotropic clays. In summary, this contribution is to firstly and comprehensively investigate the effect of anisotropic shear strengths with linear increases with depth for both the stability of planar and circular trapdoors under axisymmetric conditions. Another one is to develop a hybrid strategy to assess the stability of buried structures in soils.

A series of parametric studies were carried out to explore the effects of cover ratio (H/D), dimensionless strength gradient (m), and anisotropic strength ratio (r_e) on the stability number [N_{PS} or $N_{AX} = (\sigma_s + \gamma H - \sigma_t)/s_{uc0}$] and the associated active failure mechanisms of planar and circular trapdoors. It was shown that the stability number increases nonlinearly with H/D and r_e, while it increases linearly with m. The investigation of a shape factor ($F = N_{AX}/N_{PS}$) indicated that both strength anisotropy and heterogeneity are governing the stability differences between planar and circular trapdoors. This is particularly important for shallow buried structures. The failure patterns of trapdoors in anisotropic and non-homogeneous clays change from the vertical slip surfaces (shallow trapdoor) to the curvilinear (deep trapdoor). In this evolution process, more clays are involved in collapse zones (plastic zones) to resist the driving forces. It was noted that, however, the effect of anisotropy on the active failure mechanisms is practically insignificant.

To provide a guideline for the preliminary design of trapdoor problems, the sensitivity assessment of three dimensionless design parameters on the stability number was performed using the MARS model. Both the RII and two accurate design equations were proposed for practical uses. The sensitivity study showed that the cover ratio (H/D) and strength gradient of clays (m) are equally important in the evaluation of the stability number; nevertheless, the anisotropic strength ratio (r_e) has the least importance.

The present active trapdoor problems are studied under plane strain and axisymmetric conditions, which cover the most practical problems such as the collapse of underground roofs, tunnels, pipes, pile-supported embankments, and lateral pressures behind soil gaps in contiguous pile walls. Although the problem considered is 2D, future work in more realistic 3D trapdoor problems considering the anisotropy and heterogeneity effects of covered soils is recommended.

Availability of data and material

All of the data and models that support the findings of this study are available from the corresponding author upon request.

Declaration of competing interest

The authors declare that they have no known competing financial interests or personal relationships that could have appeared to influence the work reported in this paper.

Acknowledgments

The authors are appreciative of the funding support provided by National Natural Science Foundation of China (Grant No. 42177121), Thammasat University Research Unit in Structural and Foundation Engineering.

Appendix A. Supplementary data

Supplementary data to this article can be found online at https://doi.org/10.1016/j.jrmge.2022.07.006.

References

Al-Naddaf, M., Han, J., 2021. Spring-based trapdoor tests investigating soil arching stability in embankment fill under localized surface loading. J. Geotech. Geoenviron. Eng. 147 (9), 04021087.
Al Heib, M., Emeriault, F., Nghiem, H.L., 2020. On the use of 1g physical models for ground movements and soil-structure interaction problems. J. Rock Mech. Geotech. Eng. 12 (1), 197–211.
Azarafza, M., Ghazifard, A., Akgun, H., Asghari-Kaljahi, E., 2019. Geotechnical characteristics and empirical geo-engineering relations of the South Pars Zone marls, Iran. Geomech. Eng. 19 (5), 393–405.
Bhattacharya, P., Kumar, J., 2016. Uplift capacity of anchors in layered sand using finite-element limit analysis: formulation and results. Int. J. GeoMech. 16 (3), 04015078.
Bishop, A.W., 1966. The strength of soils as engineering materials. Geotechnique 16 (2), 91–130.
Chen, F.W., Miao, G.J., Lai, F.W., 2020. Base instability triggered by hydraulic uplift of pit-in-pit braced excavations in soft clay overlying a confined aquifer. KSCE J. Civ. Eng. 24 (6), 1717–1730.
Chen, W.F., Liu, X.L., 1990. Limit Analysis in Soil Mechanics. Elsevier, Amsterdam.
Chu, Z.F., Wu, Z.J., Liu, Q.S., Liu, B.G., Sun, J.L., 2021. Analytical solution for lined circular tunnels in deep viscoelastic burgers rock considering the longitudinal discontinuous excavation and sequential installation of liners. J. Eng. Mech. 147 (4), 04021009.
Ciria, H., Peraire, J., Bonet, J., 2008. Mesh adaptive computation of upper and lower bounds in limit analysis. Int. J. Numer. Methods Eng. 75 (8), 899–944.
Costa, Y.D., Zornberg, J.G., 2020. Active and passive arching stresses outside a deep trapdoor. Acta Geotech 15 (11), 3211–3227.
Costa, Y.D., Zornberg, J.G., Bueno, B.S., Costa, C.L., 2009. Failure mechanisms in sand over a deep active trapdoor. J. Geotech. Geoenviron. Eng. 135 (11), 1741–1753.
Davis, E.H., Christian, J.T., 1971. Bearing capacity of anisotropic cohesive soil. J. Soil Mech. Found Div. 97 (5), 753–769.
Drucker, D.C., Prager, W., Greenberg, H.J., 1952. Extended limit design theorems for continuous media. Q. Appl. Math. 9 (4), 381–389.
Friedman, J.H., 1991. Multivariate adaptive regression splines. Ann. Stat. 19 (1), 1–67.
Guan, K., Zhu, W.C., Niu, L.L., Wang, Q.Y., 2017. Three-dimensional upper bound limit analysis of supported cavity roof with arbitrary profile in Hoek-Brown rock mass. Tunn. Undergr. Space Technol. 69, 147–154.
Hwang, J.H., Kikumoto, M., Kishida, K., Kimura, M., 2005. Dynamic stability of multi-arch culvert tunnel using 3D FEM. Tunn. Undergr. Space Technol. 21 (3–4), 384.

Iglesia, G.R., Einstein, H.H., Whitman, R.V., 2011. Validation of centrifuge model scaling for soil systems via trapdoor tests. J. Geotech. Geoenviron. Eng. 137 (11), 1075–1089.
Iglesia, G.R., Einstein, H.H., Whitman, R.V., 2014. Investigation of soil arching with centrifuge tests. J. Geotech. Geoenviron. Eng. 140 (2), 04013005.
Keawsawasvong, S., Shiau, J., 2022. Stability of active trapdoors in axisymmetry. Undergr. Space 7 (1), 50–57.
Keawsawasvong, S., Ukritchon, B., 2017. Undrained stability of an active planar trapdoor in non-homogeneous clays with a linear increase of strength with depth. Comput. Geotech. 81, 284–293.
Keawsawasvong, S., Ukritchon, B., 2019. Undrained stability of a spherical cavity in cohesive soils using finite element limit analysis. J. Rock Mech. Geotech. Eng. 11 (6), 1274–1285.
Keawsawasvong, S., Ukritchon, B., 2020. Design equation for stability of shallow unlined circular tunnels in Hoek-Brown rock masses. Bull. Eng. Geol. Environ. 79, 4167–4190.
Keawsawasvong, S., Ukritchon, B., 2021. Undrained stability of plane strain active trapdoors in anisotropic and non-homogeneous clays. Tunn. Undergr. Space Technol. 107, 103628.
Keawsawasvong, S., Ukritchon, B., 2022. Design equation for stability of a circular tunnel in anisotropic and heterogeneous clay. Undergr. Space 7 (1), 76–93.
Krabbenhøft, K., 2021. Undrained failure criteria for isotropic and anisotropic soils. J. Eng. Mech. 147 (8), 06021004.
Krabbenhøft, K., Galindo-Torres, S.A., Zhang, X., Krabbenhøft, J., 2019. AUS: anisotropic undrained shear strength model for clays. Int. J. Numer. Methods Eng. 43 (17), 2652–2666.
Krabbenhøft, K., Lyamin, A.V., 2015. Generalised Tresca criterion for undrained total stress analysis. Géotech. Lett. 5 (4), 313–317.
Krabbenhøft, K., Lyamin, A.V., Krabbenhøft, J., 2015. Optum Computational Engineering (OptumG2). Available on: www.optumce.com.
Ladd, C.C., 1991. Stability evaluation during staged construction. J. Geotech. Eng. 117 (4), 540–615.
Ladd, C.C., DeGroot, D.J., 2004. Recommended Practice for Soft Ground Site Characterization: Arthur Casagrande Lecture. Massachusetts Institute of Technology.
Lai, F.W., Chen, F.Q., Li, D.Y., 2018. Bearing capacity characteristics and failure modes of low geosynthetic-reinforced embankments overlying voids. Int. J. GeoMech. 18 (8), 04018085.
Lai, F.W., Chen, S.X., Xue, J.F., Chen, F.Q., 2020. New analytical solutions for shallow cohesive soils overlying trench voids under various slip surfaces. Transp. Geotech. 25, 100411.
Lai, F.W., Zhang, N.N., Liu, S.Y., Sun, Y.X., Li, Y.L., 2021. Ground movements induced by installation of twin large diameter deeply-buried caissons: 3D numerical modeling. Acta Geotech 16 (9), 2933–2961.
Lai, F.W., Yang, D.Y., Liu, S.Y., Zhang, H.B., Cheng, Y.H., 2022. Towards an improved analytical framework to estimate active earth pressure in narrow c–soils behind rotating walls about the base. Comput. Geotech. 141, 104544.
Man, J.H., Zhou, M.L., Zhang, D.M., Huang, H.W., Chen, J.Y., 2022. Face stability analysis of circular tunnels in layered rock masses using the upper bound theorem. J. Rock Mech. Geotech. Eng. https://doi.org/10.1016/j.jrmge.2021.12.023.
Martin, C.M., 2009. Undrained collapse of a shallow plane-strain trapdoor. Geotechnique 59 (10), 855–863.
Nguyen, H.C., Nguyen-Son, L., 2022. A stable CS-FEM for the static and seismic stability of a single square tunnel in the soil where the shear strength increases linearly with depth. J. Rock Mech. Geotech. Eng. https://doi.org/10.1016/j.jrmge.2022.01.006.
Oberhollenzer, S., Tschuchnigg, F., Schweiger, H.F., 2018. Finite element analyses of slope stability problems using non-associated plasticity. J. Rock Mech. Geotech. Eng. 10 (6), 1091–1101.
Rui, R., Han, J., Van Eekelen, S., Wan, Y., 2019. Experimental investigation of soil-arching development in unreinforced and geosynthetic-reinforced pile-supported embankments. J. Geotech. Geoenviron. Eng. 145 (1), 04018103.
Shiau, J.S., Hassan, M.M., 2021a. Numerical investigation of undrained trapdoors in three dimensions. Int. J. Geosynth. Ground Eng. 7 (2), 1–12.
Shiau, J.S., Hassan, M.M., 2021b. Numerical modelling of three-dimensional sinkhole stability using finite different method. Innov. Infrastruct. So 6 (4), 1–9.
Shiau, J., Chudal, B., Mahalingasivam, K., Keawsawasvong, S., 2021a. Pipeline burst-related ground stability in blowout condition. Transp. Geotech. 29, 100587.
Shiau, J., Lee, J.S., Al-Asadi, F., 2021b. Three-dimensional stability analysis of active and passive trapdoors. Tunn. Undergr. Space Technol. 107, 103635.
Shiau, J., Keawsawasvong, S., Lee, J.S., 2022. Three-dimensional stability investigation of trapdoors in collapse and blowout conditions. Int. J. GeoMech. 22 (4), 04022007.
Sloan, S., 2013. Geotechnical stability analysis. Geotechnique 63 (7), 531–571.
Sloan, S., Assadi, A., Purushothaman, N., 1990. Undrained stability of a trapdoor. Geotechnique 40 (1), 45–62.
Suchowerska, A.M., Merifield, R.S., Carter, J.P., Clausen, J., 2012. Prediction of underground cavity roof collapse using the Hoek–Brown failure criterion. Comput. Geotech. 44, 93–103.
Tanaka, T., Sakai, T., 1993. Progressive failure and scale effect of trap-door problems with granular materials. Soils Found. 33 (1), 11–22.
Terzaghi, K., 1936. Stress distribution in dry and in saturated sand above a yielding trap-door. In: Proceeding of the First International Conference on Soil Mechanics and Foundation Engineering. Harvard University, Cambridge, Mass., USA.
Terzaghi, K., 1943. Theoretical Soil Mechanics. Wiley, New York.
Tohidifar, H., Jafari, M.K., Moosavi, M., 2021. Downwards force–displacement response of buried pipelines during dip–slip faulting in sandy soil. Can. Geotech. J. 58 (3), 377–397.
Ukritchon, B., Keawsawasvong, S., 2018a. Lower bound limit analysis of an anisotropic undrained strength criterion using second-order cone programming. J. Rock Mech. Geotech. 42 (8), 1016–1033.
Ukritchon, B., Keawsawasvong, S., 2018b. A new design equation for drained stability of conical slopes in cohesive-frictional soils. J. Rock Mech. Geotech. Eng. 10 (2), 358–366.
Ukritchon, B., Keawsawasvong, S., 2019a. Design equations of uplift capacity of circular piles in sands. Appl. Ocean Res. 90, 101844.
Ukritchon, B., Keawsawasvong, S., 2019b. Lower bound solutions for undrained face stability of plane strain tunnel headings in anisotropic and non-homogeneous clays. Comput. Geotech. 112, 204–217.
Ukritchon, B., Keawsawasvong, S., 2019c. Three-dimensional lower bound finite element limit analysis of an anisotropic undrained strength criterion using second-order cone programming. Comput. Geotech. 106, 327–344.
Ukritchon, B., Keawsawasvong, S., 2020. Undrained lower bound solutions for end bearing capacity of shallow circular piles in non-homogeneous and anisotropic clays. Int. J. Numer. Methods Eng. 44 (5), 596–632.
Ukritchon, B., Yoang, S., Keawsawasvong, S., 2019. Three-dimensional stability analysis of the collapse pressure on flexible pavements over rectangular trapdoors. Transp. Geotech. 21, 100277.
Wang, L.H., Leshchinsky, B., Evans, T.M., Xie, Y.G., 2017. Active and passive arching stresses in c′-φ′ soils: a sensitivity study using computational limit analysis. Comput. Geotech. 84, 47–57.
Won, J.Y., 2013. Anistropic strength ratio and plasticity index of natural clays. In: Proceedings of the 18th International Conference on Soil Mechanics and Geotechnical Engineering, pp. 445–448. Paris.
Wu, Z.J., Fan, L.F., Liu, Q.S., Ma, G.W., 2017. Micro-mechanical modeling of the macro-mechanical response and fracture behavior of rock using the numerical manifold method. Eng. Geol. 225, 49–60.
Wu, Z.J., Wei, R.L., Chu, Z.F., Liu, Q.S., 2021. Real-time rock mass condition prediction with TBM tunneling big data using a novel rock–machine mutual feedback perception method. J. Rock Mech. Geotech. Eng. 13 (6), 1311–1325.
Yang, D.Y., Lai, F.W., Liu, S.Y., 2022. Earth pressure in narrow cohesive-fictional soils behind retaining walls rotated about the top: an analytical approach. Comput. Geotech. 149, 104849.
Zhang, W.G., 2020. MARS Applications in Geotechnical Engineering Systems. Springer, Beijing.
Zhang, W.G., Zhang, Y.M., Goh, A.T.C., 2017. Multivariate adaptive regression splines for inverse analysis of soil and wall properties in braced excavation. Tunn. Undergr. Space Technol. 64, 24–33.
Zheng, G., Zhan, W.B., Zhou, H.Z., Yang, P.B., 2020. Multivariate adaptive regression splines model for prediction of the liquefaction-induced settlement of shallow foundations. Soil Dynam. Earthq. Eng. 132, 106097.
Zhou, T., Tian, Y.H., Cassidy, M.J., 2018. Effect of tension on the combined loading failure envelope of a pipeline on soft clay seabed. Int. J. GeoMech. 18 (10), 04018131.
Zhou, H.Z., Xu, H.J., Yu, X.X., et al., 2021. Evaluation of the bending failure of columns under an embankment loading. Int. J. GeoMech. 21 (7), 040211.

Jim Shiau is currently Associate Professor at University of Southern Queensland, Australia. He received a PhD degree from University of Newcastle, NSW, Australia where he continued two years of post-doctorate under the leadership of late Laureate Professor Scott Sloan. His research focuses on deep braced excavation and soft ground tunneling, sinkhole stability, finite element limit and shakedown analyses for geotechnical stability problems. Jim Shiau has extensive experience in the design of underground structures. He enjoys the breadth of general practice with interests in geotechnical stability research. He has published more than 15 high-impact Q1 journal articles as both first and corresponding authors. Jim Shiau has also involved in the organization of several international conferences in Australia since 2014.